Direct Observation of Molecular Preorganization for Chirality Transfer on a Catalyst Surface

Vincent Demers-Carpentier, *et al.*

Science **334**, 776 (2011);
DOI: 10.1126/science.1208710

perspectives for highly sensitive measurements with a new generation of atom interferometers.

Bücker *et al*. (*34*) recently reported reduced atom number fluctuations in twin-atom beams, and the group of M. Oberthaler has independently used spin dynamics in Bose-Einstein condensates to generate atomic two-mode entanglement detected by a homodyning technique.

References and Notes

1. N. F. Ramsey, *Phys. Rev.* **78**, 695 (1950).
2. C. Bordé, *Phys. Lett. A* **140**, 10 (1989).
3. L. Essen, J. V. L. Parry, *Nature* **176**, 280 (1955).
4. R. Wynands, S. Weyers, *Metrologia* **42**, S64 (2005).
5. G. Santarelli *et al*., *Phys. Rev. Lett.* **82**, 4619 (1999).
6. L. Pezzé, A. Smerzi, *Phys. Rev. Lett.* **102**, 100401 (2009).
7. J. Appel *et al*., *Proc. Natl. Acad. Sci. U.S.A.* **106**, 10960 (2009).
8. J. Estève, C. Gross, A. Weller, S. Giovanazzi, M. K. Oberthaler, *Nature* **455**, 1216 (2008).
9. C. Gross, T. Zibold, E. Nicklas, J. Estève, M. K. Oberthaler, *Nature* **464**, 1165 (2010).
10. I. D. Leroux, M. H. Schleier-Smith, V. Vuletić, *Phys. Rev. Lett.* **104**, 073602 (2010).
11. M. F. Riedel *et al*., *Nature* **464**, 1170 (2010).
12. Z. Chen, J. G. Bohnet, S. R. Sankar, J. Dai, J. K. Thompson, *Phys. Rev. Lett.* **106**, 133601 (2011).
13. J. J. Bollinger, W. M. Itano, D. J. Wineland, D. J. Heinzen, *Phys. Rev. A* **54**, R4649 (1996).
14. M. J. Holland, K. Burnett, *Phys. Rev. Lett.* **71**, 1355 (1993).
15. A. Kuzmich, L. Mandel, *Quantum Semiclass. Opt.* **10**, 493 (1998).
16. Z. Y. Ou, J.-K. Rhee, L. J. Wang, *Phys. Rev. Lett.* **83**, 959 (1999).
17. P. Walther *et al*., *Nature* **429**, 158 (2004).
18. M. W. Mitchell, J. S. Lundeen, A. M. Steinberg, *Nature* **429**, 161 (2004).
19. I. Afek, O. Ambar, Y. Silberberg, *Science* **328**, 879 (2010).
20. V. Meyer *et al*., *Phys. Rev. Lett.* **86**, 5870 (2001).
21. D. Leibfried *et al*., *Nature* **438**, 639 (2005).
22. L.-M. Duan, A. Sørensen, J. I. Cirac, P. Zoller, *Phys. Rev. Lett.* **85**, 3991 (2000).
23. H. Pu, P. Meystre, *Phys. Rev. Lett.* **85**, 3987 (2000).
24. T. Kim, O. Pfister, M. J. Holland, J. Noh, J. L. Hall, *Phys. Rev. A* **57**, 4004 (1998).
25. T. Nagata, R. Okamoto, J. L. O'brien, K. Sasaki, S. Takeuchi, *Science* **316**, 726 (2007).
26. C. Klempt *et al*., *Phys. Rev. Lett.* **104**, 195303 (2010).
27. S. M. Barnett, D. T. Pegg, *Phys. Rev. A* **42**, 6713 (1990).
28. M. Scherer *et al*., *Phys. Rev. Lett.* **105**, 135302 (2010).
29. Supporting material is available on *Science* Online.
30. C. Klempt *et al*., *Phys. Rev. Lett.* **103**, 195302 (2009).
31. R. A. Campos, B. E. A. Saleh, M. C. Teich, *Phys. Rev. A* **40**, 1371 (1989).
32. P. Hyllus, L. Pezzé, A. Smerzi, *Phys. Rev. Lett.* **105**, 120501 (2010).
33. P. Hyllus, O. Gühne, A. Smerzi, *Phys. Rev. A* **82**, 012337 (2010).
34. R. Bücker *et al*., *Nat. Phys.* **7**, 608 (2011).

Acknowledgments: We thank E. Rasel for stimulating discussions and P. Zoller for helpful comments. We acknowledge support from the Centre for Quantum Engineering and Space-Time Research (QUEST), the European Science Foundation (EuroQUASAR), and the Danish National Research Foundation Center for Quantum Optics. P.H. acknowledges financial support of the European Research Council Starting Grant GEDENTQOPT. This work was supported in part by Provincia Autonoma di Trento within the activities of the BEC center. L.P. acknowledges support by the Laboratoire Charles Fabry de L'Institut d' Optique where part of this work was completed.

Supporting Online Material

www.sciencemag.org/cgi/content/full/science.1208798/DC1
SOM Text
Figs. S1 to S5
References (*35*–*40*)

23 May 2011; accepted 23 September 2011
Published online 13 October 2011;
10.1126/science.1208798

Direct Observation of Molecular Preorganization for Chirality Transfer on a Catalyst Surface

Vincent Demers-Carpentier,[1] Guillaume Goubert,[1] Federico Masini,[1] Raphael Lafleur-Lambert,[1] Yi Dong,[1] Stéphane Lavoie,[1] Gautier Mahieu,[1] John Boukouvalas,[1] Haili Gao,[2] Anton M. H. Rasmussen,[2] Lara Ferrighi,[2] Yunxiang Pan,[2] Bjørk Hammer,[2]* Peter H. McBreen[1]*

The chemisorption of specific optically active compounds on metal surfaces can create catalytically active chirality transfer sites. However, the mechanism through which these sites bias the stereoselectivity of reactions (typically hydrogenations) is generally assumed to be so complex that continued progress in the area is uncertain. We show that the investigation of heterogeneous asymmetric induction with single-site resolution sufficient to distinguish stereochemical conformations at the submolecular level is finally accessible. A combination of scanning tunneling microscopy and density functional theory calculations reveals the stereodirecting forces governing preorganization into precise chiral modifier-substrate bimolecular surface complexes. The study shows that the chiral modifier induces prochiral switching on the surface and that different prochiral ratios prevail at different submolecular binding sites on the modifier at the reaction temperature.

Chirality transfer and amplification on surfaces is fundamentally important to progress in the synthesis of enantiopure compounds for pharmaceutical and agrochemical applications (*1*–*4*) and to discussions of the origin of biological homochirality (*5*). Chirally modified heterogeneous catalysts, in which the reaction is stereocontrolled at surface sites formed by adsorbing a chiral molecule, offer a number of sought-after advantages, including ease of separation of the catalyst from the product. The best-explored examples in terms of potential applications involve the hydrogenation of activated ketones to chiral alcohols and hydroxy esters on cinchona-modified Pt (*6*, *7*). A number of synthetic modifiers that share some key structural and functional characteristics of cinchonidine, such as 1-(1-naphthyl)ethylamine (NEA) and its condensation derivatives (*8*), can also be used. However, a lack of mechanistic understanding has long been seen as an impediment to the rational development of chirally modified heterogeneous catalysts (*6*, *7*).

We directly characterized the surface complexation of a prochiral reagent with a chiral modifier by using 2,2,2-trifluoroacetophenone, TFAP, as the prochiral substrate, (*R*)-(+)-NEA as the modifier, and Pt(111) as the metal surface. Preorganization in this chemisorption system can be described in terms of molecular recognition between a fully chiral molecule and a molecule that is chiral only by virtue of its confinement on the surface (*4*, *9*–*15*). The experiment resolves interactions at the level of functional groups at individual modifier sites and thereby provides insight into the structural preorganization that biases the stereochemical outcome of the reaction, in essence the mechanism of chirality transfer. The scanning tunneling microscopy (STM) measurements were carried out at room temperature in parallel with room temperature catalytic measurements on the asymmetric hydrogenation of TFAP to 2,2,2-trifluorophenylethanol over (*R*)-NEA modified Pt on an alumina support.

The interactions of the chiral modifier and the prochiral substrate with the metal surface were first studied separately. Two modifier motifs, present in a 7:3 ratio, are observed in the STM images (Fig. 1, A and B). The two motifs may be distinguished by the position of the bright protrusion: It extends from the central region of the image in the majority motif (A) and from the left-hand side in the minority motif (B). The two lowest energy structures predicted by density functional theory (DFT) are the (*R*)-NEA-1 and (*R*)-NEA-2 conformers (Fig. 1, E and F). Their calculated adsorption energies are ~2 eV with a pronounced 0.13 eV preference for the (*R*)-NEA-1 conformation (figs. S10 and S11), suggesting that their relative surface coverages are determined in part by adsorption dynamics. Surface vibrational spectroscopy measurements (figs. S1 and S2) confirm that the NEA conformers are chemisorbed in the geometry found in the DFT calculations. In particular, the C-CH_3 bond is nearly perpendicular to the surface, as also described for the Pd(111) surface (*16*).

[1]Centre de recherche sur les propriétés des interfaces et la catalyse (CERPIC) and Département de chimie, Université Laval, Québec, QC G1V 0A6, Canada. [2]Interdisciplinary Nanoscience Center (iNANO) and Department of Physics and Astronomy, Aarhus University, DK 8000 Aarhus, Denmark.

*To whom correspondence should be addressed. E-mail: hammer@phys.au.dk (B.H.); peter.mcbreen@chm.ulaval.ca (P.H.M.)

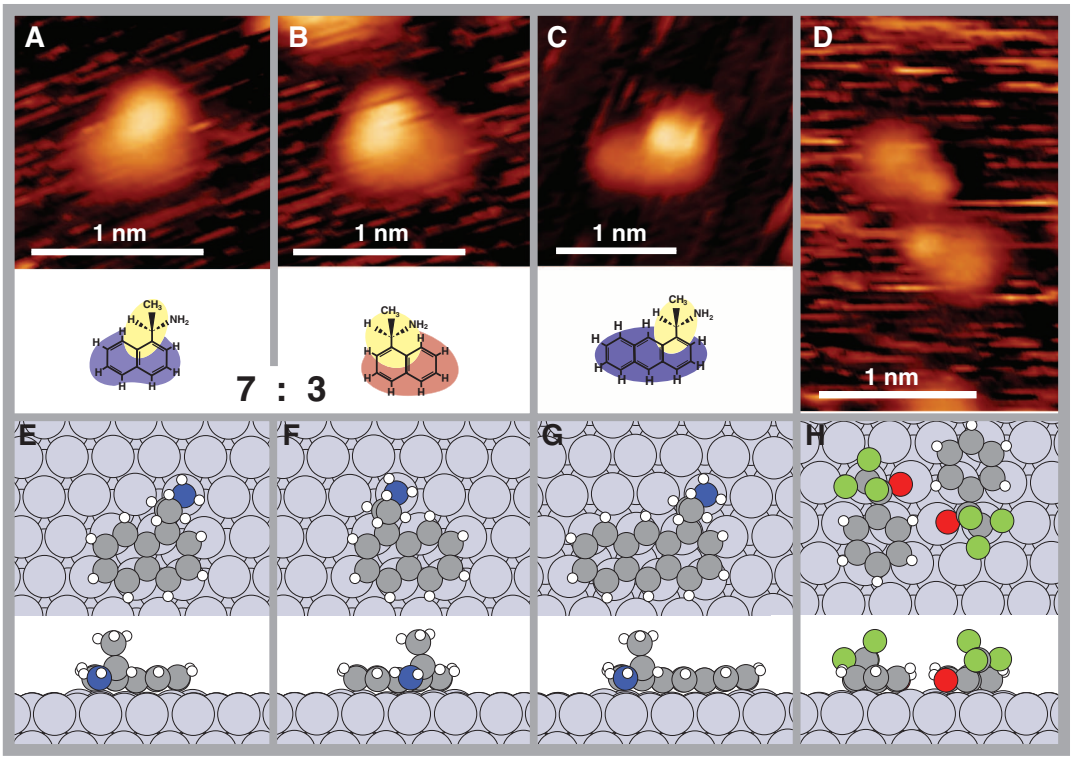

Fig. 1. STM images and DFT-calculated structures of the single enantiomer modifier, (*R*)-NEA, and the prochiral substrate, TFAP, chemisorbed separately on Pt(111) at room temperature. The modifier, (*R*)-(+)-1-(1-naphthyl)ethylamine, is imaged in two distinct forms in a 7-to-3 ratio. These two conformations [(**A**) and (**B**)], (*R*)-NEA-1 and (*R*)-NEA-2, differ in whether the NH_2 group points to the edge or the center of the two-ring aromatic framework [(**E**) and (**F**)]. The STM image (**C**) and DFT-calculated structure (**G**) of 1-(1-anthryl)ethylamine are used to identify the bright protrusion as the ethylamine group. Chemisorption of the substrate, 2,2,2-trifluoroacetophenone, leads to the formation of homochiral dimers (*17*). A pro-*S* dimer and the corresponding calculated structure are shown in (**D**) and (**H**), respectively. STM images were recorded at room temperature, 1.2-V sample bias, and 0.3-nA tunnel current.

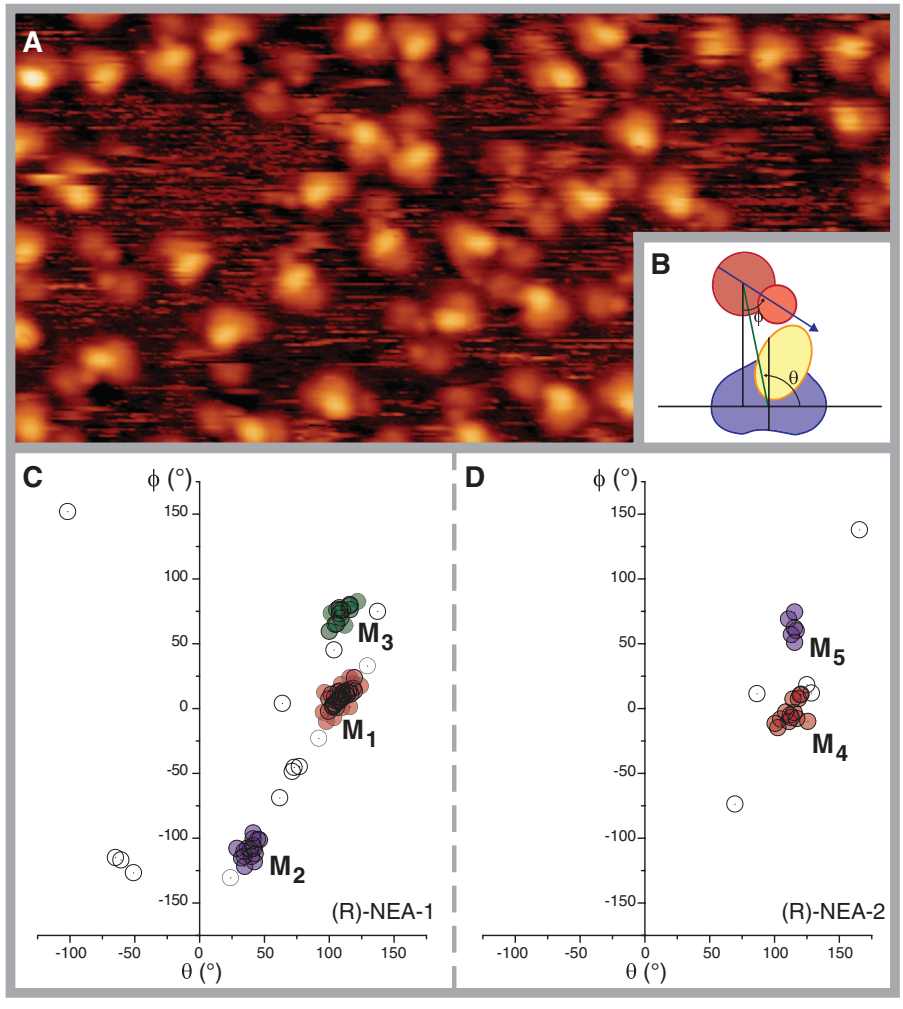

Fig. 2. STM image of the chemisorption system formed by adding TFAP to (*R*)-NEA–modified Pt(111). (**A**) Large scan (11.5 nm by 5.5 nm) image, taken with the sample held at room temperature, shows that TFAP forms both dimers and modifier-substrate complexes. The distribution of geometries in the diastereomeric complexes, as determined from a visual inspection, is plotted in (**C**) and (**D**) in terms of the angular position (θ) and orientation (ϕ) of TFAP with respect to (*R*)-NEA, as defined in (**B**). A color code is used to emphasize the existence of five distinct abundant families, three (M_1 to M_3) involving (*R*)-NEA-1 and two (M_4 and M_5) involving (*R*)-NEA-2. STM images were recorded at 1.2-V bias and 0.3-nA current.

Upon chemisorption, the substrate forms dimers, and each TFAP is imaged (Fig. 1D) as a bowling-pin motif in which the small brighter protrusion is caused by the trifluoroacetyl substituent. DFT calculations predict a binding energy of ~1 eV per TFAP monomer and suggest that dimers are stabilized (*17*) by two simultaneous aryl-CH···OC interactions in a homochiral conformation (Fig. 1H). Because the DFT calculations establish the directionality of the carbonyl groups within each dimer, the prochirality of dimerized TFAP can be determined by a visual inspection of the STM images. Pro-*S* dimers are shown in Fig. 1, D and H, and additional examples of pro-*R* and pro-*S* dimers are presented in fig. S6. In keeping with the objective of chirality transfer to the hydrogenation product, the pro-*S* configuration is defined as the one that would yield (*S*)-2,2,2-trifluorophenylethanol following attack by adsorbed atomic hydrogen at the enantioface in direct contact with the metal surface.

When both the modifier and the substrate are present on the surface, STM images taken at room temperature show a dynamic system where, in addition to forming dimers, TFAP binds to (*R*)-NEA. Video measurements (movie S1) reveal that the dimers disassemble and reassemble on the time scale of the experiment and that individual TFAP molecules form short-lived complexes (seconds to a few minutes) with the modifier. The ratio of (*R*)-NEA-1 to (*R*)-NEA-2 is conserved upon adding the substrate. At the coverage used in this study, about 60% of the NEAs are interacting with a TFAP molecule at any given time. A visual inspection of these modifier-substrate complexes in terms of TFAP's angular position (θ) and orientation (ϕ) with respect to the modifier (as defined in Fig. 2B) shows tight groupings of the experimental structures into five distinct geometries (M_1 to M_5; Fig. 2, C and D). The corresponding STM motifs are shown in Fig. 3. By using DFT calculations (Fig. 3 and figs. S17 and S18), we explored the best possible (*R*)-NEA+TFAP complexes on the Pt surface. Three of the four most stable (*R*)-NEA-1+TFAP complexes and the two most stable (*R*)-NEA-2+TFAP complexes found by DFT are included in Fig. 3. These calculated structures match with the five most abundant families observed by STM both in terms of the location of the TFAP around the ethylamine group and the direction in which it points (see fig. S19 for simulated STM images). We note that one additional rather stable

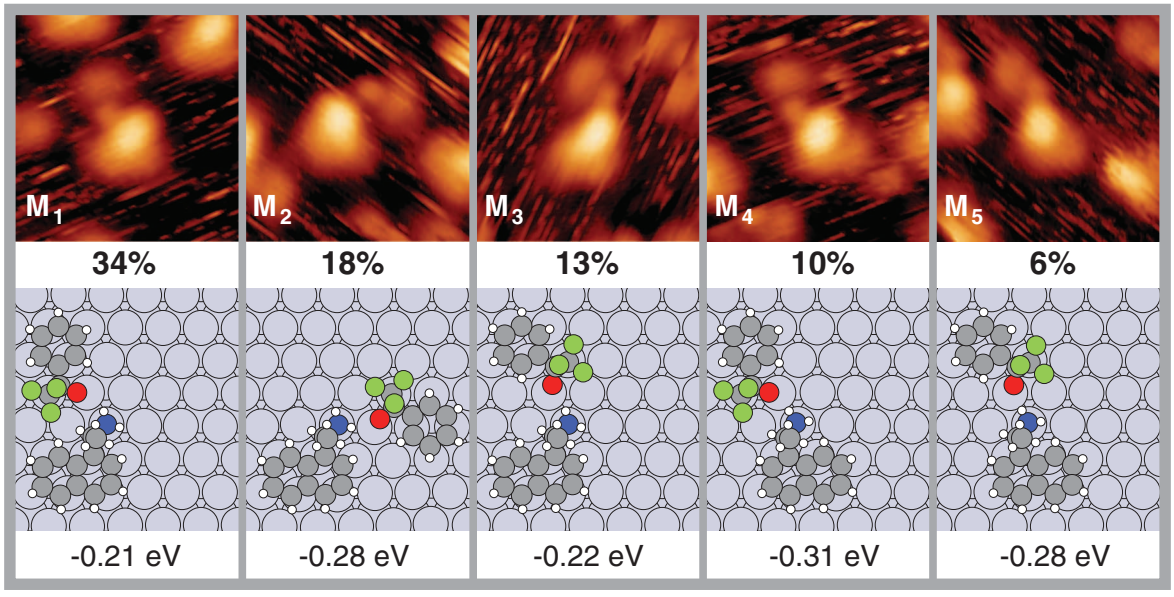

Fig. 3. STM images and DFT-calculated structures of the five most frequently observed modifier-substrate diastereomeric complexes, M_1 to M_5. The indicated percentages are relative to the total population of 900 complexes. The DFT-calculated structures establish the prochirality of the substrate in families M_1 to M_5. The numbers below the calculated structures are the potential energies relative to the separated substrate and modifier (figs. S16 and S19). STM images were recorded at a 1.2-V bias and 0.3-nA tunnel current, with the sample at room temperature.

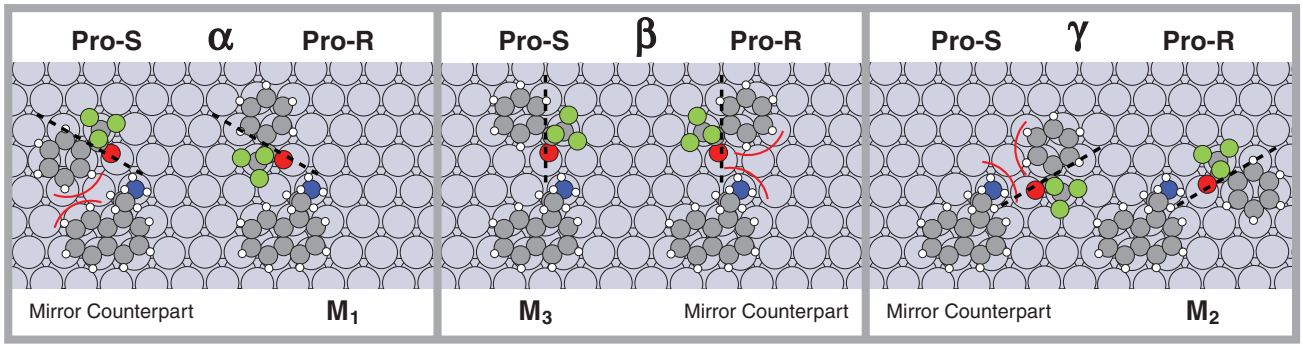

Fig. 4. DFT-calculated structures for mirror-image complexes formed by binding TFAP to (*R*)-NEA-1 on Pt(111). For each binding site (α, β, and γ), two stable complexes of inverse prochirality are found. Dashed lines indicate the mirror planes perpendicular to the surface that bring pro-*R* TFAP into pro-*S* TFAP and vice versa. For example, by taking the M_3 family (left-hand side of the middle panel) where a pro-*S* TFAP binds at the top of the ethylamine group [β-(*S*)], a reflection operation relative to the dashed line gives the mirror counterpart [β-(*R*)]. The same symmetry operation applied to all of the M_i groups [plus a possible γ-(*R*) species for (*R*)-NEA-2] reveals the 12 families used for the statistical analysis presented in Fig. 5. Red arcs indicate stereodirecting repulsive interactions for the low population families. According to the energy calculations, the mirror counterparts are about 0.1 to 0.3 eV less stable (fig. S20).

(*R*)-NEA-1+TFAP complex is identified with DFT (complex X_1 in fig. S17) but does not correspond to any of the abundant families observed in the STM images, suggesting that it undergoes facile conversion into one of the observed structures. The excellent overall correspondence between experiment and theory allows us to discuss the imaged complexes in terms of the calculated structures. In particular, it reveals that the five most abundant families all form via NH_2···OC interactions. Hence, the prochirality of TFAP substrate in each of the complexes can be determined by visual inspection of the STM images.

Labeling the five most abundant families in terms of the combination of the prochirality of TFAP (pro-*R* or pro-*S*) and the position where it binds to the ethylamine function (α, β, and γ for the left-hand, top, and right-hand sites, respectively) gives α-(*R*) for M_1 and M_4, β-(*S*) for M_3 and M_5, and γ-(*R*) for M_2. It then becomes natural to look for less abundant families as complexes of inverse TFAP prochirality at the given sites, that is, to look for α-(*S*), β-(*R*), and γ-(*S*) families (Fig. 4). It turns out that ~93% of all complexes in a sample of 900 can be accounted for by including the less abundant mirror-image families. The remaining nonassigned complexes consist mainly of TFAP interacting with the naphthyl ($\theta < 0$ data points, Fig. 2C) instead of the ethylamine group and complexes resulting from high local coverage. Termolecular complexes of one (*R*)-NEA and two TFAPs are observed where both the α and γ sites are simultaneously occupied (fig. S5), implying that the ethylamine group is in the same conformation for both binding events, in agreement with the DFT calculations (Fig. 3, M_1 and M_2).

A statistical analysis of over 900 complexes (Fig. 5) shows that we are observing a strong expression of regiospecific prochiral differentiation. For example, the most frequently observed complex is formed by pro-*R* TFAP at the α position of (*R*)-NEA-1 corresponding to family M_1 (Figs. 2 and 3). It accounts for 34% of all of the complexes, whereas its pro-*S* counterpart accounts for 3%. This 11-to-1 pro-*R*–to–pro-*S* ratio is evidence of strong prochiral steering at the α site. Further, 1-to-6 and 6-to-1 pro-*R*–to–pro-*S* ratios are measured at the β and γ sites, respectively. The overall stereoselectivity of (*R*)-NEA-1 is good, with a ratio of 3 to 1 (obtained from adding the TFAP populations at all three binding sites for this conformer), whereas for (*R*)-NEA-2 a less-pronounced 3-to-2 ratio is observed.

In order to test the actual enantioselectivity of (*R*)-NEA–modified Pt for TFAP hydrogenation, we carried out catalytic measurements using Pt/Al_2O_3 at room temperature. Indeed, enantioselection is observed with an enantiomeric excess of ~34% (corresponding to an enantiomeric ratio of roughly 2:1) in favor of the (*R*)-product. This moderate expression of asymmetry is in line with our STM measurements on (*R*)-NEA–modified Pt(111), also at room temperature, identifying predominantly pro-*R* preorganization and a smaller but significant fraction of pro-*S* preorganization.

The classification of STM images, calculated structures, and energies (Figs. 3 and 5) gives detailed information on the diastereomeric complexes inducing chirality transfer from the modifier to the substrate. The DFT calculations (Fig. 4) reveal that the observed prochiral excesses can be explained by the balance between an attractive NH···OC interaction and a simple set of repulsive forces in the low population families α-(*S*), β-(*R*), and γ-(*S*). Simulation of the coadsorption of (*R*)-NEA-1 and trifluoromethyl 2-pyridyl ketone to form β-(*R*) and β-(*S*) complexes evens out the energy difference between the two prochiralities (fig. S21), revealing that a repulsive interaction between the amine group of the modifier and the phenyl moiety of TFAP is the reason for the low populations of β-(*R*) and γ-(*S*) families. Similarly, the α-(*S*) family is disfavored relative to α-(*R*) because of steric interaction between the phenyl group of the substrate and the naphthyl group of the modifier. Phenyl-naphthyl repulsion also causes the absence of a γ-(*R*)/(*R*)-NEA-2 family. Our observations thus identify repulsive interactions with the phenyl group as the main stereodirecting force at the origin of the enantioselectivity for the NEA-TFAP pair. This subtle steric effect occurs in the presence of the binding NH_2···OC interaction and the yet stronger chemisorption interaction of TFAP.

Importantly for a chirality transfer process (*18*, *19*), the relative abundances of TFAP surface enantiomers averaged over ensembles of coexisting TFAP dimers and TFAP/(*R*)-NEA complexes reveal that the modifier induces prochiral switching of the adsorbed substrate. There is an overall excess of pro-*R* TFAP that increases with the coverage of the modifier. Symmetry breaking is observed to occur irrespective of the sequence in which the substrate and the modifier are added to the surface. When the surface is first exposed to TFAP and then to (*R*)-NEA to a surface coverage of roughly 1/3 monolayer of (*R*)-NEA and 1/3 monolayer of TFAP (as shown in Fig. 2), a pro-*R* excess up to 15 ± 2% is observed. For experiments performed by first adsorbing (*R*)-NEA

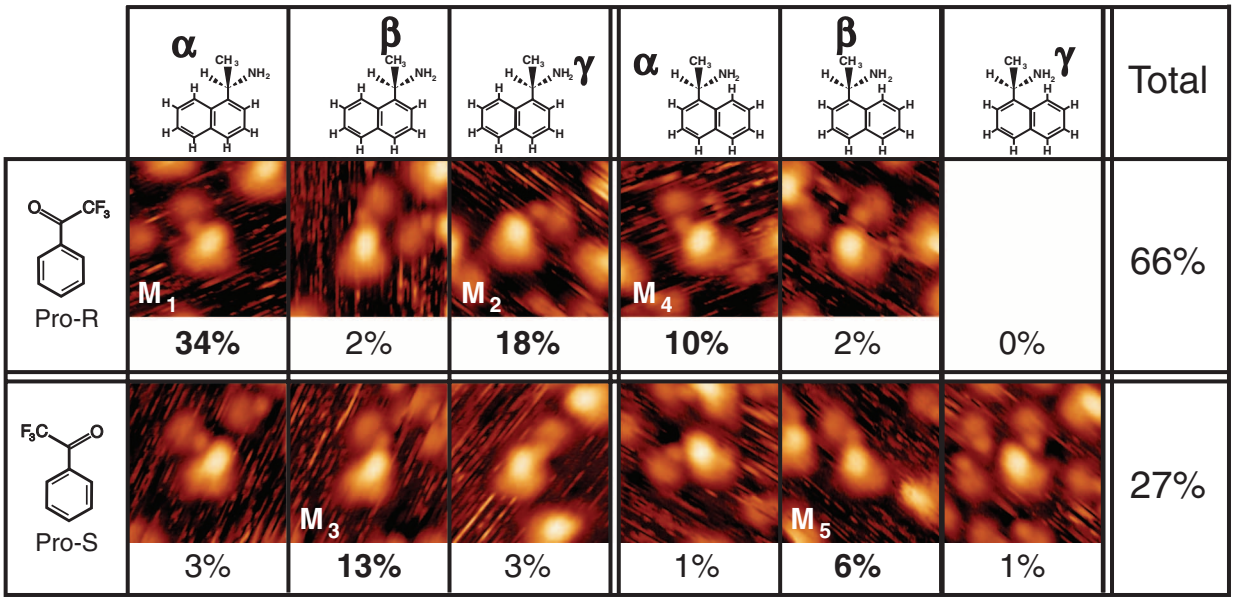

Fig. 5. Classification of 900 modifier-substrate complexes formed by (*R*)-NEA and TFAP on Pt(111) at room temperature into distinct stereochemical and regiochemical arrangements. Each entry shows a 2 nm–by–2 nm STM image of an archetypal complex of a particular family, along with the percentage of the total complex population it represents. The remaining 7% mostly consist of complexes where TFAP binds to the naphthyl instead of the ethylamine group and irregularly shaped complexes likely caused by high local coverages. STM images were recorded at a 1.2-V bias and 0.3-nA current with the sample at room temperature.

and then dosing TFAP on the modified surface with similar coverages, pro-*R* excesses of up to 16 ± 3% are observed. This behavior can be explained simply by low barrier rotation of the trifluoroacetyl group followed by preferential capture of pro-*R* TFAP to form diastereomeric complexes at free binding sites around the ethylamine group of the modifier. The observed symmetry breaking is a direct manifestation of the action of (*R*)-NEA as a chiral modifier of the Pt(111) surface.

The previous lack of direct information on modifier-substrate stereodirecting interactions has been the major roadblock in the comprehension and optimization of chirally modified heterogeneous asymmetric catalysts. As this study demonstrates, efficient stereodirection occurs through subtle energy differences in the presence of stronger ones, including chemisorption bonding. It is extraordinarily difficult to identify the origin of these differences, and their relative importance, in the absence of direct measurements. The combination of STM and DFT used here to describe chirality transfer preorganization in terms of regiospecific prochiral ratios is a key step forward. It can serve as a basis for profound studies of the kinetic relevance of individual submolecular sites as well as for studies of the stereodynamics of heterogeneous asymmetric induction. Our model-free analysis suggests that for the NEA-TFAP pair a higher enantiomeric excess could be achieved by molecular design to limit the chiral pocket to one binding site, rather than the multiple sites observed. Efforts could be directed toward blocking the counterproductive β site and/or favoring chemisorption of NEA-1 over the less-selective NEA-2 conformer. In future work, STM/DFT-guided asymmetric catalyst design could be applied to other modifier substrate pairs and a broader range of reactions.

References and Notes

1. G. Kyriakou, S. K. Beaumont, R. M. Lambert, *Langmuir* **27**, 9687 (2011).
2. M. Forster, M. S. Dyer, M. Persson, R. Raval, *Top. Catal.* **54**, 13 (2011).
3. A. J. Gellman, *ACS Nano* **4**, 5 (2010).
4. A. G. Trant, C. J. Baddeley, *J. Phys. Chem. C* **115**, 1025 (2011).
5. K. H. Ernst, *Orig. Life Evol. Biosph.* **40**, 41 (2010).
6. H.-U. Blaser, M. Studer, *Acc. Chem. Res.* **40**, 1348 (2007).
7. M. Heitbaum, F. Glorius, I. Escher, *Angew. Chem. Int. Ed.* **45**, 4732 (2006).
8. E. Orglmeister, T. Mallat, A. Baiker, *Adv. Synth. Catal.* **347**, 78 (2005).
9. J. M. Bonello, F. J. Williams, R. M. Lambert, *J. Am. Chem. Soc.* **125**, 2723 (2003).
10. Q. Chen, N. V. Richardson, *Nat. Mater.* **2**, 324 (2003).
11. S. Weigelt *et al.*, *Nat. Mater.* **5**, 112 (2006).
12. A. Kühnle, T. R. Linderoth, B. Hammer, F. Besenbacher, *Nature* **415**, 891 (2002).
13. L. Ning, S. Haq, G. R. Darling, R. Raval, *Angew. Chem. Int. Ed.* **40**, 7613 (2007).
14. M. Lingenfelder *et al.*, *Angew. Chem. Int. Ed.* **46**, 4492 (2007).
15. S. Blankenburg, W. G. Schmidt, *Phys. Rev. Lett.* **99**, 196107 (2007).
16. L. Burkholder, M. Garvey, M. Weinert, W. T. Tysoe, *J. Phys. Chem. C* **115**, 8790 (2011).
17. V. Demers-Carpentier *et al.*, *J. Phys. Chem. C* **115**, 1355 (2011).
18. R. R. Knowles, E. N. Jacobsen, *Proc. Natl. Acad. Sci. U.S.A.* **107**, 20678 (2010).
19. A. Zehnacker, M. A. Suhm, *Angew. Chem. Int. Ed.* **47**, 6970 (2008).

Acknowledgments: This work was supported by a Natural Sciences and Engineering Research Council of Canada (NSERC) discovery grant, a Fonds Québécois de la Recherche sur la Nature et les Technologies (FQRNT) team grant, Canadian Foundation for Innovation (CFI) grants, and the FQRNT Centre in Green Chemistry and Catalysis (CCVC). This work was in part supported by the Lundbeck Foundation, the Danish Research Councils, and the Danish Center for Scientific Computing. V.D.-C. acknowledges an NSERC graduate student scholarship.

Supporting Online Material

www.sciencemag.org/cgi/content/full/334/6057/776/DC1
Materials and Methods
SOM Text
Figs. S1 to S19
Tables S1 to S4
References (*20*–*38*)
Movie S1

20 May 2011; accepted 19 September 2011
10.1126/science.1208710

N_2 Reduction and Hydrogenation to Ammonia by a Molecular Iron-Potassium Complex

Meghan M. Rodriguez,[1] Eckhard Bill,[2] William W. Brennessel,[1] Patrick L. Holland[1]*

The most common catalyst in the Haber-Bosch process for the hydrogenation of dinitrogen (N_2) to ammonia (NH_3) is an iron surface promoted with potassium cations (K^+), but soluble iron complexes have neither reduced the N-N bond of N_2 to nitride (N^{3-}) nor produced large amounts of NH_3 from N_2. We report a molecular iron complex that reacts with N_2 and a potassium reductant to give a complex with two nitrides, which are bound to iron and potassium cations. The product has a Fe_3N_2 core, implying that three iron atoms cooperate to break the N-N triple bond through a six-electron reduction. The nitride complex reacts with acid and with H_2 to give substantial yields of N_2-derived ammonia. These reactions, although not yet catalytic, give structural and spectroscopic insight into N_2 cleavage and N-H bond-forming reactions of iron.

The Haber-Bosch process is a large-scale method for catalytic reduction of dinitrogen (N_2) with dihydrogen (H_2) to give ammonia (NH_3). This process is vital for production of synthetic fertilizer, which is needed to produce food for the world's expanding population (*1*). Several metals catalyze the Haber-Bosch process (iron, ruthenium, osmium, uranium, and cobalt-molybdenum), but iron has received the most industrial and theoretical attention because of its hardiness and low cost (*2*–*4*). The most common iron catalyst is promoted by K^+ additives and was developed by Mittasch in 1910 (*2*). In the century since then, chemists have studied the nature of active iron and iron/potassium surfaces, as well as the kinetics of N_2 reduction (*3*). These studies have shown that iron is predominantly in the zero oxidation state in the catalyst. Importantly, the rate-limiting step of the catalytic process is N_2 chemisorption and N-N bond cleavage to give surface-bound nitrides (N^{3-}), which react with H_2 to form the N-H bonds in NH_3 (Fig. 1). However, many details of the bond-breaking and bond-forming steps are difficult to discern by using surface science techniques, for example, how many iron atoms are involved in the N-N dissociation step and whether the K^+ promoter interacts with N_2 during the N-N dissociation step (*4*). Similar uncertainties surround postulated mechanisms for N_2 reduction by nitrogenase enzymes, which have iron (in the +2 and +3 oxidation states) at their active sites (*5*, *6*).

Reactions of iron coordination compounds with N_2 are of interest because the products can shed light on Fe-N_2 interactions in atomic detail. Although the behavior of iron atoms in a coordination compound (where they have a positive formal charge) is inevitably different than the zero valent iron atoms on a metallic surface, coordination compounds are more amenable to detailed structural characterization. Unfortunately, iron coordination complexes are poor at reduc-

[1]Department of Chemistry, University of Rochester, Rochester, NY 14627, USA. [2]Max-Planck-Institut für Bioanorganische Chemie, Stiftstrasse 34-36, D-45470 Mülheim an der Ruhr, Germany.

*To whom correspondence should be addressed. E-mail: holland@chem.rochester.edu

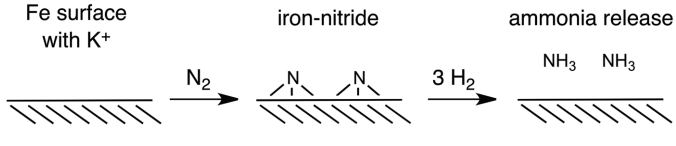

Fig. 1. Simplified scheme of the ammonia formation pathway in the Haber-Bosch process.